FEBS Letters

FEBS PRESS science publishing by scientists

RESEARCH LETTER

Expanding the antiviral potential of the mosquito lipid-transfer protein AEG12 against SARS-CoV-2 using hydrophobic antiviral ligands

Alexander C. Y. Foo[1], Bernard A. P. Lafont[2] and Geoffrey A. Mueller[1]

1 Genome Integrity and Structural Biology Laboratory, National Institute of Environmental Health Sciences, Research Triangle Park, NC, USA

2 SARS-CoV-2 Virology Core, Laboratory of Viral Diseases, National Institute of Allergy and Infectious Diseases, Bethesda, MD, USA

Correspondence

G. A. Mueller, Genome Integrity and Structural Biology Laboratory, National Institute of Environmental Health Sciences, MRI 018, 111 T.W. Alexander Dr., Research Triangle Park, NC 27709, USA

Tel: 984-287-3589

E-mail: mueller3@niehs.nih.gov

(Received 26 May 2022, revised 13 July 2022, accepted 15 July 2022, available online 4 August 2022)

doi:10.1002/1873-3468.14456

Edited by Urs Greber

The mosquito protein AEG12 encompasses a large (~ 3800 Å^3) hydrophobic cavity which binds and delivers unsaturated fatty acids into biological membranes, allowing it to lyse cells and neutralize a wide range of enveloped viruses. Herein, the lytic and antiviral activities are modified with non-naturally occurring lipid ligands. We generated novel AEG12 complexes in which the endogenous fatty acid ligands were replaced with hydrophobic viral inhibitors. The resulting compounds modulated cytotoxicity and infectivity against SARS-CoV-2, potentially reflecting additional mechanisms of action beyond membrane destabilization. These studies provide valuable insight into the design of novel broad-spectrum antiviral therapeutics centred on the AEG12 protein scaffold as a delivery vehicle for hydrophobic therapeutic compounds.

Keywords: antiviral; drug delivery; enveloped virus; lipid-binding protein; membrane disruption; SARS-CoV-2

The mosquito protein AEG12 is a member of the insect major allergen (MA) domain protein family which has been implicated in both insect digestion and antiviral defense [1–5]. The MA fold consists of 12 amphipathic alpha-helices, which enclose a large hydrophobic cavity [6–8]. This hydrophobic cavity can bind a range of hydrophobic ligands. Previous work on the cockroach MA protein Bla g 1 revealed a mixture of saturated and unsaturated fatty acids – particularly palmitate, oleate and stearate – as the endogenous (nMix) ligands when extracted from cockroach frass, with additional evidence suggesting that these lipids likely represent the native cargo of other MA proteins such as AEG12 [6–8]. In these studies, both Bla g 1 and AEG12 were shown to mediate the delivery of these nMix ligands into biological membranes, disrupting their biophysical structure. This activity enables AEG12 to inhibit the infectivity of enveloped viruses such as flaviviruses, lentiviruses and coronaviruses, contributing to its antiviral function within the mosquito and potentially providing the basis for the design of novel antiviral compounds [6]. However, the membrane destabilizing properties of AEG12's natural nMix ligands also allow it to lyse mammalian cells [6]. While this cell cytotoxicity likely facilitates digestion within the insect midgut, it significantly limits the utility of AEG12 as a human therapeutic.

Abbreviations

CD, circular dichroism; Doc, docosanol; DPPC, dipalmitoyl-phosphatidylcholine; DSPC, distearoylphosphatidylcholine; GA, ginkgolic acid (15:1); GP, generalized polarization; HEK, human embryonic kidney; LAURDAN, dodecanoyl-*N*,*N*-dimethyl-2- naphthylamine; LPC, 16:0 lysophosphatidylcholine; MA, major allergen; MT, melting temperature; nsLTP, non-specific lipid transfer protein; PC, phosphatidylcholine; PE, phosphatidylethanolamine; PT, phase-transition temperature; R18, octadecyl rhodamine B chloride; SARS-CoV-2, severe acute respiratory syndrome coronavirus 2.

Major allergen proteins are distinguishable by the large size (~ 3800 $Å^3$) of its central hydrophobic cavity: dwarfing the 100–500 $Å^3$ range typical of most non-specific lipid-transfer proteins (nsLTPs) [7,9–11]. This allows MA proteins such as AEG12 to support an exceptionally high binding stoichiometry of 8–12 fatty acid ligands per protein molecule – equivalent to ~ 10% w/w [6,8]. This large cavity also enables MA proteins to accommodate a large range of non-natural ligands, providing a convenient avenue that might enhance the therapeutic utility of AEG12-derived protein scaffolds [12]. Recent work has identified several such compounds including ginkgolic acid (GA), lysophosphatidylcholine and docosanal [13–17]. These compounds have been shown to effectively inhibit a broad range of enveloped viruses including influenza, HIV and coronaviruses *in vitro* by modifying the structure and biophysical properties of the viral lipid envelope. However, their lipophilic nature limits their solubility while making them extremely susceptible to sequestration by non-specific lipid-binding proteins such as serum albumins, reducing their therapeutic utility.

Replacing the nMix ligands of AEG12 with non-natural viral inhibitors such as the ones described above could address the inherent limitations of both these systems. In this work, we loaded AEG12 with docosanol (Doc), 16:0-lysophosphatidylcholine (LPC) and GA ligands. AEG12 mediated delivery of these non-natural ligands into model bilayer systems. While cytotoxicity was retained under some conditions, all three AEG12 complexes showed a significant increase in therapeutic index over their natural fatty-acid-loaded counterparts reflecting their more specialized function. Encapsulating these fusion inhibitors within the AEG12 scaffold had the additional benefit of enhancing their solubility compared to the free ligands while simultaneously protecting them from interference and sequestration by albumins and other serum factors. Together, these studies provide valuable insight into the development of novel therapeutic strategies leveraging the unique lipid delivery capabilities of AEG12 and other MA proteins to facilitate the delivery of hydrophobic antiviral compounds directly into biological membranes.

Methods

Expression, purification and biophysical characterization of AEG12

Samples of AEG12 were prepared as described previously [6,12]. In brief, AEG12 was expressed as a glutathione-*S*-transferase (GST) fusion in *Escherichia coli*. The resulting protein was purified using affinity chromatography, and the GST tag was cleaved using TEV protease. The resulting AEG12 protein was further purified using reverse-phase high-performance liquid chromatography and re-folded either in the Apo (empty) form or in the presence of the appropriate fusion inhibitor [6,7,12]. Protein concentrations were determined using the Bicinchoninic Acid Assay kit (Pierce, Waltham, MA, USA). Amberlite-treated samples were generated using 30 $mg{\cdot}mL^{-1}$ of Amberlite Resin (Sigma, St. Louis, MO, USA) per mg of lipid ligand. Following a 1–2 h incubation at room temperature, the beads were removed and protein concentration was confirmed as described above. Thermodenaturation curves were collected using a Jasco J-815 circular dichroism (CD) spectropolarimeter (Iola, KS, USA). 0.5 μM samples of AEG12 in CD buffer (100 mM Tris pH 7.5, 50 mM NaCl) were loaded into 10 mm quartz cuvettes, and the CD at 220 nm was measured over a range of temperatures from 25 °C to 95 °C at a heating rate of 0.5 $°C{\cdot}min^{-1}$. Measurements were taken every 2 °C and fit using a two-state Boltzmann curve to determine the melting temperature (MT): defined as the temperature at which the protein experienced a 25% loss in secondary structure as described previously [6].

Assessing the biological activity of AEG12 *in vitro*

Vesicle membrane fusion was assessed using an R18 dilution assay. Here, dipalmitoylphosphatidylcholine (DPPC) vesicles containing 5 mol% octadecyl rhodamine B chloride (R18; Thermo Fisher, Waltham, MA, USA) were prepared using a lipid extruder with a 1.0 μm membrane (Avanti, Birmingham, AL, USA) as per manufacturer's instructions. Unlabelled DPPC vesicles were prepared in a similar fashion. The influenza fusion peptide (GLFGAIAGFIENGWEGMIDG) [18] was synthesized by Genscript (Piscataway, NJ, USA), and resuspended in DMSO to a final concentration of 2 mM. Unlabelled vesicles (10 $mg{\cdot}mL^{-1}$) were incubated with 25 μM AEG12 for 1 h, and washed three times in PBS to remove excess AEG12 and any unbound ligands. 22.5 μL of unlabelled vesicles were then resuspended in 240 μL citrate buffer (100 mM citrate pH 5.4). The fusion reaction was initiated by the addition of 2.5 μL of R18-labelled vesicles and 7.5 μL of influenza fusion peptide to yield a final concentration of 0.1 $mg{\cdot}mL^{-1}$ lipid vesicles (1 : 10 labelled to unlabelled) and 33 μM fusion peptide. R18 is a fluorophore (ex_{560}, em_{590}) that self-quenches at high concentrations [19]. The effective local concentration of R18 is significantly reduced upon fusion with an unlabelled vesicle, resulting in an increase in fluorescence intensity [20]. R18 fluorescence intensity was monitored over the course of 15 min and used to quantify the rate of vesicle fusion. Positive (no AEG12) and negative (no AEG12, no fusion peptide) controls were also carried out. Experimental values were normalized, with the positive control (no AEG12) being set to 100%, in order to obtain relative rates of vesicle fusion.

Vesicle stability measurements were carried out as described previously [6]. In brief, distearoylphosphatidylcholine (DSPC) vesicles were prepared as described above. A 3.70 mg·mL^{-1} solution of DSPC vesicles was resuspended in PBS and incubated in the presence of 2 μM LAURDAN (Sigma) and 25 μM AEG12 for 1 h at 37 °C. The resulting mixture was diluted 10-fold and placed in a 2 mL quartz cuvette. Fluorescence spectra (ex_{355}, $em_{400–500}$) were collected at 2 °C increments from 24 °C to 88 °C using a Fluoromax-Plus-CP-Spectrophotometer (Horiba, Kyoto, Japan) at a heating rate of 2 °C·min^{-1}. Generalized polarization (GP) values were calculated using the fluorescence intensity at 440 and 490 nm [21]. The resulting GP values were fit to a two-state Boltzmann equation to calculate the phase-transition temperature (PT).

AEG12 cell cytotoxicity and antiviral activity

The cytotoxic activity of AEG12 was assessed using techniques described previously [6]. In brief, human embryonic kidney (HEK) cells were suspended in PBS to a final concentration of 1×10^6 cells·mL^{-1} in the absence or presence of 10% FBS. The cells were incubated with increasing concentrations of Doc-AEG12 (0–150 μM), GA-AEG12 (0–75 μM) or LPC-AEG12 (0–75 μM) for 37 °C for 1 h. The resulting mixture was diluted 1 : 1 with acridine orange/propidium iodide stain solution (Nexcelom, Lawrence, MA, USA). Cells were imaged as per manufacturer's recommended protocols using a Zeiss AxioObserver Z1 fluorescence microscope (Carl Zeiss Incorporated, Oberkochen, Germany) at 10× magnification. The images were analysed using FIJI/IMAGEJ [22], and the resulting cell viability values were fit to an exponential decay function to obtain cytotoxicity (CC_{50}) values – defined as the concentration of AEG12/inhibitor which yields a 50% reduction in cell viability relative to the negative control (PBS only). To determine the CC_{50} values of the free ligand, LPC and GA stocks were prepared in PBS and diluted to the appropriate concentration, taking into account the expected 8 : 1 binding stoichiometry of AEG12.

Antiviral activity was assessed using a plaque reduction assay as described previously [23]. Here, samples of SARS-COV-2/USA-WA1/2020 (35–40 PFU per 100 μL) were incubated for 1 h at 37 °C in DMEM containing 2% FBS and varying the concentration of the appropriate AEG12–inhibitor complexes. Vero cells overexpressing TMPRSS2 (Vero-T2), a gift from the laboratory of Jonathan Yewdell (NIAID), were grown in 12-well plates at 37 °C at 5% CO_2 in D10+ medium [DMEM + 10% FBS, 1× Glutamax, 1× Anti-Anti (Gibco, Waltham, MA, USA) and 250 μg·mL^{-1} Hydromycin B (InVivoGen, San Diego, CA, USA)] to a density of 0.4×10^6 cells/well. Cells were washed twice with D2 medium (DMEM + 2% FBS and 1× Glutamax) and inoculated with the AEG12–virus mixture for 1 h at 37 °C. At the end of the absorption step, the cell monolayers were overlaid with DMEM medium containing 0.6% methylcellulose and incubated for 3 days at 37 °C. The cell monolayers were stained and fixed with crystal violet staining solution containing 5% ethanol and 3% neutral buffered formalin for 20 min, and then washed with water to visualize the viral plaques. Viral plaques were counted manually, and the resulting data were fit to an exponential decay function to determine IC_{50} values. The IC_{50} values were compared with the HEK cell cytotoxicity (CC_{50}) values determined in the previous sections to provide a relative assessment of the therapeutic index.

Data reporting

All values and associated uncertainty reported in this work represent the mean and standard deviation obtained from at least three trials representing at least two biological replicates unless otherwise specified.

Results

AEG12 binds and delivers hydrophobic fusion inhibitors into lipid bilayers

Previous studies described techniques through which lipid-binding proteins could be stripped of their endogenous cargoes, and quantitatively re-loaded with a defined set of hydrophobic ligands [12]. Using this technique, we prepared samples of AEG12 loaded with docosanol (Doc), 16:0-lysophosphatidylcholine (LPC) and GA: compounds that have been previously characterized in the literature as hydrophobic viral inhibitors [14–17,24,25]. Binding of all three inhibitors resulted in a notable increase in the thermostability of AEG12 relative to the Apo control, with melting temperatures (MT_{AEG12}) comparable to those observed for AEG12 bound to its natural nMix ligands (Fig. 1) [6,7]. While the unique nature of the AEG12–ligand complex precludes traditional equilibrium-based K_D measurements, the large thermal shift observed upon ligand binding is consistent with the formation of a stable, high-affinity complex that is potentially amenable for therapeutic use [6,7,26].

Previous works suggest that the incorporation of docosanol, LPC and GA into viral membranes hinders their ability to fuse with their host cell counterparts, resulting in their observed antiviral activity [13–17,25,27]. With this in mind, we examined the ability of our various AEG12 complexes to inhibit membrane fusion using DPPC lipid vesicles. Here, vesicle fusion was monitored by the dilution of the self-quenching octadecyl rhodamine B chloride (R18) fluorescent dye from labelled to unlabelled vesicles in the presence of an influenza fusion peptide at pH 5.4 [18,20]. Under these conditions, 25 μM GA-AEG12 was observed to

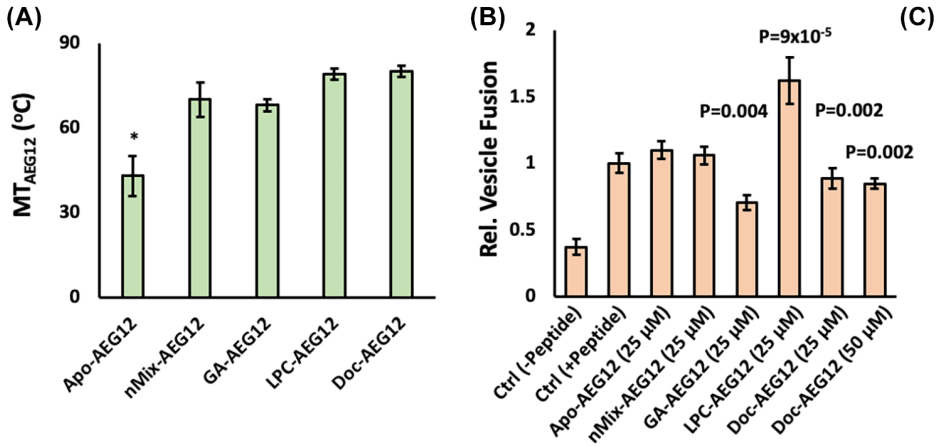

(C)

Condition	PT (°C)
PBS	55.4±0.2
Apo*	55.8±0.5
nMix-AEG12*	51.7±0.6
GA-AEG12	52.4±0.8
Free GA	50.0±0.6
LPC-AEG12	54.5±0.2
Free LPC	55.5±0.1
Doc-AEG12	56±1

Fig. 1. *In vitro* characterization of AEG12–inhibitor complexes. (A) Thermostability of AEG12 in complex with various natural and non-natural antiviral ligands measured by circular dichroism (MT). (B) Impact of AEG12 on the influenza fusion peptide-mediated fusion of octadecyl rhodamine B chloride (R18)-labelled DPPC lipid vesicles. Measurements were carried out using 25 or 50 μM complex and normalized against a positive (+peptide) control (see Methods). *P*-values for conditions that differed significantly from Apo-AEG12 were determined using a Student's *T*-test assuming equal variance. (C) Solid–liquid PT of DSPC lipid vesicles in PBS (control) or in the presence of 25 μM AEG12 or the equivalent free ligand. Note that free docosanol was not assessed due to its low solubility. *Values obtained from previously published sources [6].

significantly inhibit membrane fusion, representing a significant improvement over the Apo and nMix fatty acid-loaded species. Doc-AEG12 had a much smaller inhibitory effect, even using twofold greater concentrations than its GA-bound counterpart. Curiously, LPC-AEG12 was observed to increase the rate of membrane fusion. Other works have noticed inconsistencies in LPC's mode of antiviral activity, suggesting a more complex mechanism of action [17].

The antiviral function of the naturally occurring nMix ligands is mediated by its ability to disrupt lipid membranes [6]. This same mechanism might contribute to the antivirus activity of Doc-, LPC- and GA-loaded AEG12. To test this hypothesis, DSPC lipid vesicles were labelled with dodecanoyl-*N*,*N*-dimethyl-2-naphthylamine (LAURDAN), and incubated with 25 μM of the various AEG12–inhibitor complexes. The liquid–solid phase-transition temperature (PT) of the resulting vesicles was assessed as described previously [6], and the results are shown in Fig. 1C. GA-AEG12 yielded a noticeable reduction in PT, although the magnitude of this destabilizing effect was somewhat reduced relative to its natural nMix counterparts, potentially indicating a reduction in cell cytotoxicity. In contrast, Doc-AEG12 had no effect, suggesting a minimal impact on membrane structure. Despite its reputation as a 'harsh' detergent, LPC-AEG12 produced only a minor shift in PT. Incubating DSPC vesicles with free LPC ligands yielded similar results. Given the strong partition coefficient into lipid bilayers [28], the meagre responses observed in this assay likely represent an innate property of the LPC ligand itself. This is consistent with previous works in which the saturated acyl chain of LPC detergents had minimal impact on the packing density or phase-transition temperature of lipid membranes, despite other adverse effects [29,30].

AEG12–inhibitor complexes display enhanced therapeutic potential

The membrane-destabilizing properties of AEG12's natural nMix ligands resulted in robust cytolytic activity against mammalian cells, greatly limiting its therapeutic utility [6]. To determine whether these inhibitor-bound AEG12 species share this limitation, HEK cells were treated with varying concentrations (0–150 μM) of AEG12 for 1 h at 37 °C as described previously [6]. Doc-AEG12 had no impact on cell viability under the conditions tested, while GA-AEG12 displayed modest cytotoxic activity (Fig. 2) comparable to that previously reported for its natural nMix counterpart (Fig. 3) [6]. Curiously, the cytotoxic activity of LPC-AEG12 was significantly enhanced despite the lack of membrane destabilization observed in Fig. 1, potentially reflecting the indirect correlation between PT and membrane permeability [31,32]. Regardless of the mechanism, the conclusion is that the biological activity of our AEG12–inhibitor complexes is mediated by its bound ligand [6]. Indeed, both free LPC and GA supported significant cell cytotoxicity consistent with

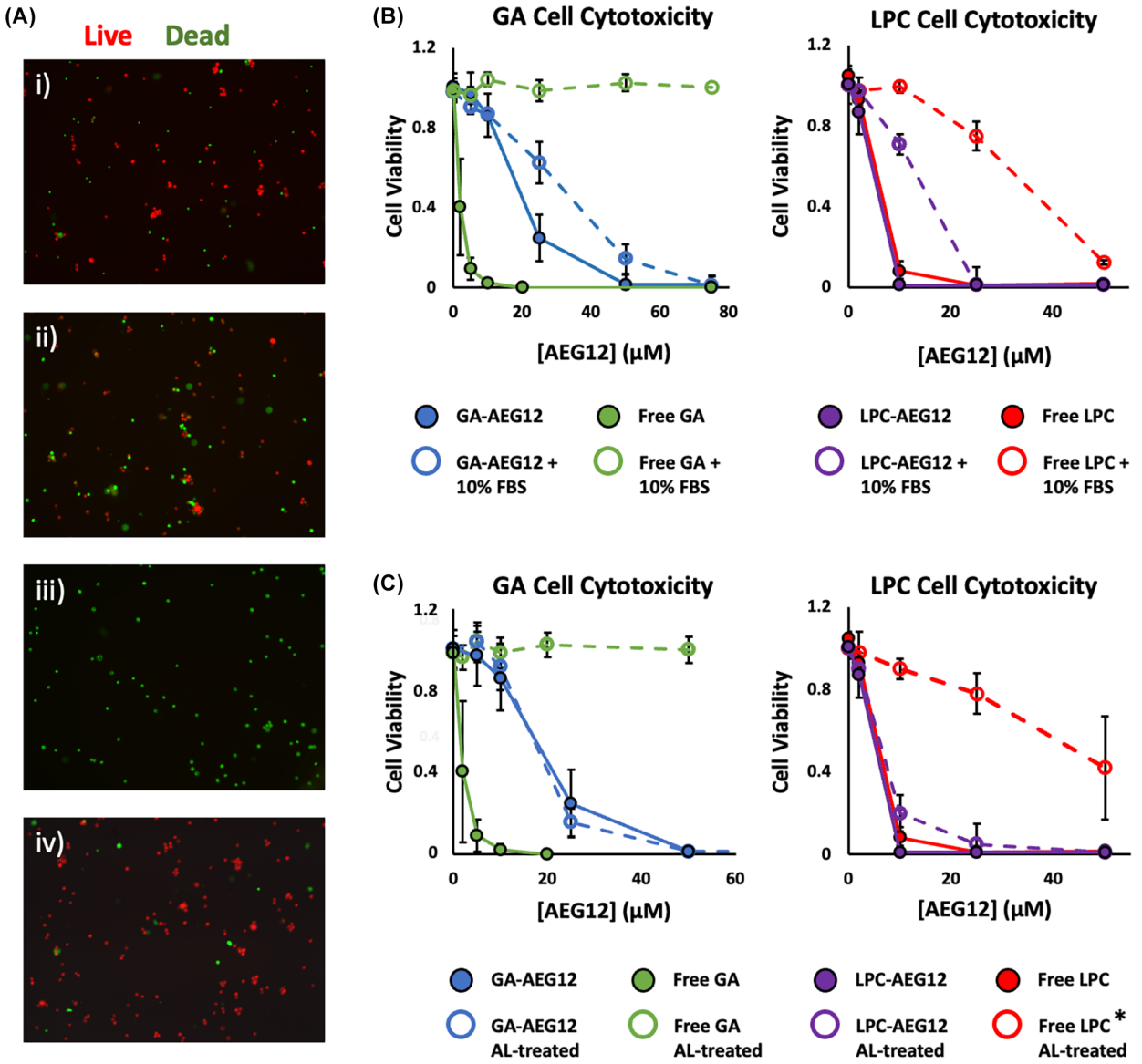

Fig. 2. Cytotoxic activity of AEG12–inhibitor complexes. (A) Cell cytotoxicity of AEG12–inhibitor complexes against HEK cells. Representative microscope images (10×) showing HEK cells following a 1 h incubation in PBS (i), in the presence of 10 μM GA-AEG12 (ii), 10 μM LPC-AEG12 (iii) or 100 μM Doc-AEG12 (iv). In this assay, live and dead cells are stained to be either red or green respectively. (B) Impact of FBS on the cytotoxic activity of free and AEG12-bound GA and LPC. (C) Impact of Amberlite resin on the cytotoxic activity of free and AEG12-bound GA and LPC. *Data obtained from two independent trials from one biological replicate.

previous literature [33]. Curiously, free GA had a lower CC_{50} than its AEG12-bound counterpart. This is potentially indicative of incomplete ligand transfer due to the high binding affinity observed in the previous section, or the larger phenolic headgroup reducing the carrying capacity relative to its nMix counterparts. Free docosanal was not tested in this assay due to its lack of cytotoxicity and the low solubility of the free ligand (< 0.1 μM).

Utility of AEG12 as a drug delivery scaffold

The cytotoxicity of GA and LPC, either as free lipids in solution or complex with AEG12, was assessed in the presence of 10% FBS to better replicate the *in vivo* environment. The cytotoxicity of both GA and LPC as free ligands was significantly reduced under these conditions, potentially reflecting their sequestration by albumins and other serum factors [34,35]. Both GA-

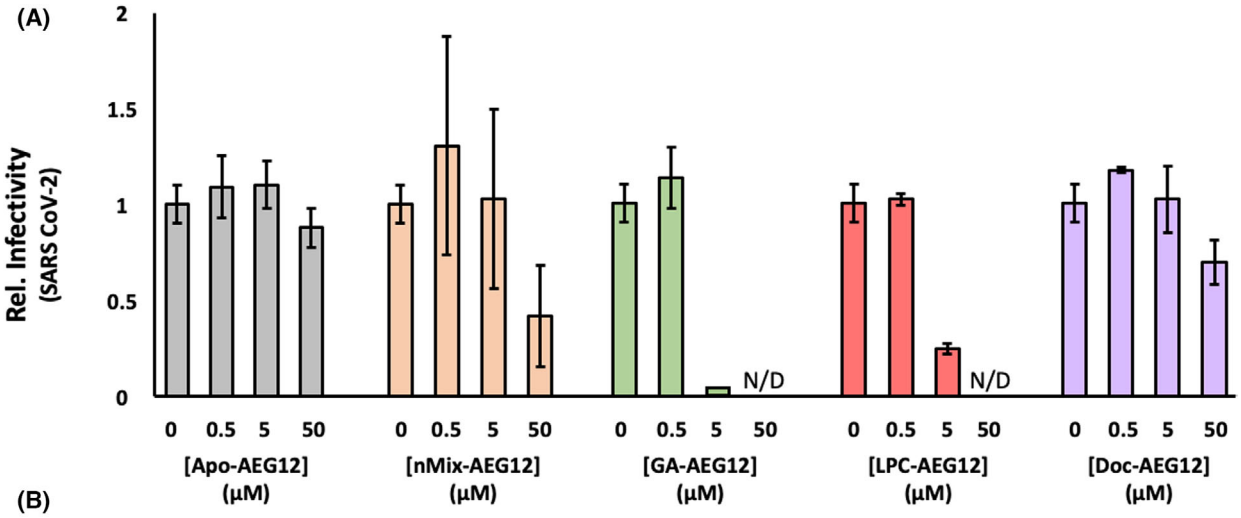

Condition	Cytotoxicity CC_{50} (μM) HEK Cells	Antiviral Activity IC_{50} (μM) SARS CoV-2	Rel. Therapeutic Index
Apo-AEG12	>100*†	>150	N/D
nMIx-AEG12	12±2*	42±15	1±0.5
GA-AEG12	14±2	2.0±0.1	26±5
LPC-AEG12	6.0±0.5	4.5±0.2	5.0±0.6
Doc-AEG12	>150†	82±8	>7

Fig. 3. Antiviral activity of AEG12–inhibitor complexes. (A) Relative infectivity of SARS CoV-2 viruses following incubation with AEG12–inhibitor complexes. Near-zero values represent conditions where no viral plaques were detected. N/D denotes conditions that were not tested due to cell cytotoxicity concerns. The therapeutic index of the various AEG12–inhibitor complexes relative to nMix-AEG12 is shown in B. *Values obtained from two independent trials representing two biological replicates. †< 20% cell cytotoxicity observed at the highest concentration tested (150 μM).

AEG12 and LPC-AEG12 experienced a minor loss of efficacy, but still retained significant biological activity (Fig. 2). Even treatment by Amberlite – a resin specifically designed to bind and sequester fatty acid ligands – failed to significantly reduce the CC_{50} of both LPC-AEG12 and GA-AEG12 (Fig. 2). As noted above and in previous studies, the biological activity of AEG12 is derived from its ability to bind and deliver hydrophobic ligands into biological membranes [6]. In this capacity, the high affinity of the AEG12–ligand complex provides a significant degree of protection from interference by albumins or other serum factors while facilitating rapid delivery upon encountering its molecular targets.

The ability of AEG12 to deliver fusion inhibitors into lipid bilayers of both host and viral membranes is expected to reduce viral infectivity. To test this hypothesis, we examined the ability of our various AEG12 complexes to inhibit SARS CoV-2, the causative agent responsible for the COVID-19 pandemic. Consistent with previous studies, the natural nMix-AEG12 complex displayed modest antiviral activity, with IC_{50} values in the mid-μM range following a 30 min incubation at 37 °C in the presence of 2% FBS (Fig. 3) [6]. Under similar conditions, the Apo form had no effect, again mirroring our previous studies. Use of the GA and LPC fusion inhibitors significantly enhanced antiviral activity with IC_{50} values approximately one order of magnitude lower than those observed using their natural nMix ligands. This resulted in a ~ 20-fold increase in the relative therapeutic index for GA-AEG12 over its nMix counterpart as calculated using the CC_{50}/IC_{50} ratio. The elevated cytotoxicity of LPC-AEG12 resulted in a more modest increase, although a significant improvement over nMix-AEG12 was still noted. The use of docosanol as an AEG12 cargo embodies the opposite approach; while Doc-AEG12 displayed markedly reduced

antiviral activity, its lack of cytotoxicity resulted in a net increase in the therapeutic index on par with LPC.

Discussion

Major allergen proteins such as AEG12 are defined by a large hydrophobic cavity that can bind a range of hydrophobic ligands. In this study, we are able to leverage this capability to facilitate the delivery of hydrophobic viral inhibitors such as GA, LPC and docosanol into biological membranes, resulting in the formation of novel antiviral inhibitors with varying degrees of cell cytotoxicity and antiviral efficacy against SARS-CoV-2. GA and LPC also retained significant membrane destabilization and cell cytotoxicity, potentially contributing to their antiviral activity. In addition to membrane destabilization, the incorporation of rigid or cone-shaped lipids, such as docosanol [16,25], ginkgolic acid [15] and lysophosphatidylcholine [17,27], has been proposed to impair the ability of viral membranes to fuse with their target host cells, providing an additional mechanism for antiviral activity [13–17]. In this work, GA-AEG12 and Doc-AEG12 may have retained this capability to varying degrees, contributing to the increase in antiviral activity relative to their cytotoxicity, although the specific molecular mechanism was not examined in this work.

Regardless of the mechanism, the biological activity of AEG12 is dependent on their bound hydrophobic ligands, with the protein itself acting primarily as a delivery vehicle. Indeed, the greatest enhancement in the therapeutic index was observed in GA-AEG12: a ligand whose ability to inhibit viral membrane fusion and infectivity has been previously documented [14,15,24]. However, these studies found that free GA interacted with serum factors such as albumins and other lipid-binding proteins, reducing its efficacy in a therapeutic setting [15]. Using AEG12 as a delivery vehicle significantly ameliorates this limitation, as the high affinity and thermodynamic stability of the AEG12-GA complex protects its cargoes from sequestration by serum factors and even specialist detergent-absorbing resins such as Amberlite. It should also be noted that the protocol for generating our AEG12–inhibitor complexes involves numerous buffer exchange and filtration steps. The ability of AEG12 to retain its bound ligands following this treatment provides further evidence for its stability and resilience, highlighting its potential utility as an *in vivo* therapeutic agent.

The concept of using lipid-binding proteins as drug delivery vehicles has been proposed previously in the literature. Early attempts focused on albumins and transferrins due to their broad substrate specificity and relatively favourable biophysical properties. However, these proteins are limited by their mechanism of action. Here, the lipid–protein interaction is defined by a typical dissociation equilibrium, with the ligand existing in either the bound form or as an aqueous monomer (Fig. 4A). Transfer of these ligands from their carrier protein into a target bilayer occurs *via* the monomeric phase and is thus dependent on the dissociation equilibrium of the lipid–protein complex. Under this model, tight binding affinities severely limit the concentration of free ligand present in solution at any given time. This prevents sequestration of the ligands by serum albumins, albeit at the cost of greatly reduced ligand delivery kinetics, with lifetimes in the hours or tens of hours observed in some studies [36,37]. As with any other lipid-protein complex, MA proteins such as AEG12 also undergo the same dissociation equilibrium shown in Fig. 4A. However, they are also able to directly exchange lipids with the target membrane *via* a membrane-bound intermediate, bypassing the need to form a monomeric species (Fig. 4B) [6]. By decoupling the two processes, the AEG12 complex is able to remain stable for hours or days in solution with limited exchange with the aqueous environment or other serum factors, yet deliver its ligands on the minute timescale upon encountering its target lipid bilayer [6]. This lipid exchange mechanism also imparts some selectivity with regards to the target membrane. For instance, Foo et al. [6] observed that AEG12-mediated ligand delivery is significantly reduced against phosphatidylethanolamine (PE) bilayers due to the reduced stability of the resulting AEG12-PE product. In contrast, AEG12 has a high affinity for phosphatidylcholine (PC) lipids, facilitating delivery against flaviviruses and coronaviruses whose bilayers contain high proportions of PC lipids [6]. This mechanism could be further developed using protein engineering approaches to impart greater control over AEG12-mediated lipid delivery: a capacity that is not possible using either the free ligands or 'equilibrium-based' protein scaffolds.

It should be noted that plant non-specific lipid transfer proteins (nsLTPs) also display a similar mode of action involving a membrane-bound intermediate state [38,39]. This allows nsLTPs to support rapid delivery kinetics similar to those observed for AEG12, while permitting low concentrations of free, monomeric ligand in solution [11,38–40]. However, these proteins are unable to match the binding stoichiometry of AEG12, with most nsLTPs being able to accommodate up to 2 fatty acids compared to the 8–10 observed for MA proteins. The correspondingly smaller size of the nsLTP hydrophobic cavity (100–500 $Å^3$)

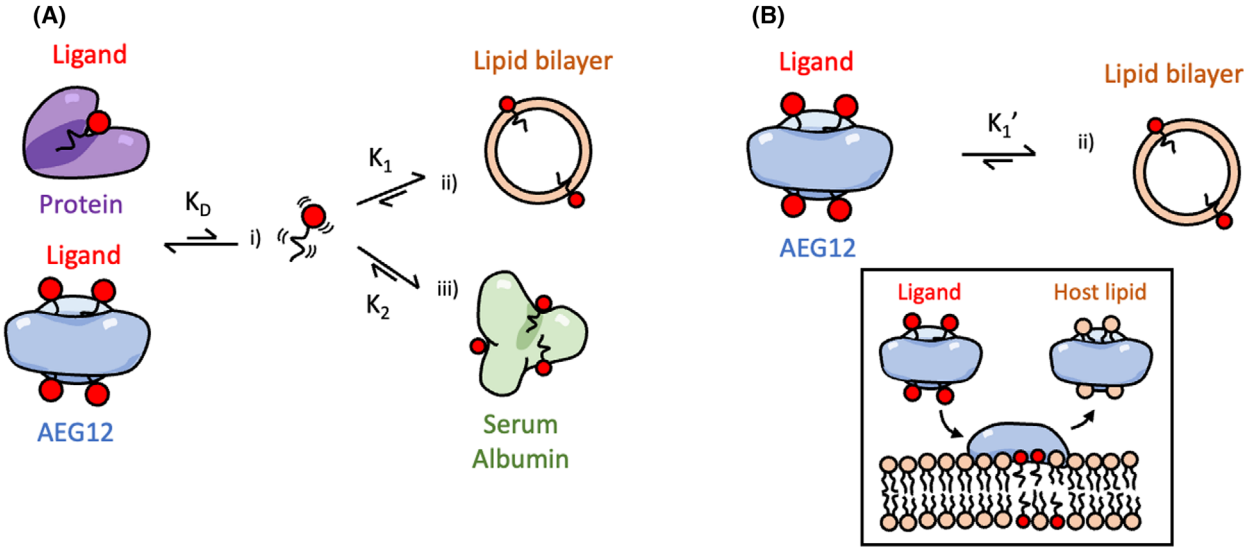

Fig. 4. Two models for protein-mediated lipid drug delivery. (A) Equilibrium model. The lipid–ligand interaction is defined by a traditional dissociation equilibrium (K_D), with the ligand existing as either in the protein-bound or free monomeric/aqueous form (i). Sequestration by serum albumins (iii) and transfer to lipid vesicles (ii) occur *via* the free monomeric form, and are thus dependent on K_D: a small K_D yields a small concentration of free ligand, protecting it from sequestration but hindering transfer to its target bilayer. Large K_D values favour the generation of the free monomeric ligand species, promoting both ligand transfer and sequestration/dissociation. (B) Direct transfer model. AEG12 binds to the target membrane (inset), where it can exchange lipids directly with the target membrane. Ligand transfer *via* this pathway (K_1') is not dependent on the generation of the free monomeric ligand (K_D), allowing AEG12 to support rapid and effective ligand transfer on the minutes timescale while retaining tight ligand-binding affinities in solution.

also restricts the types of cargoes which can be accommodated [7,9–11]. An interesting comparison can also be drawn between AEG12 and cyclodextrins. Cyclodextrins are cyclic oligosaccharides that encapsulate a hydrophobic cavity: analogous to the architecture of AEG12. Like AEG12, this large hydrophobic cavity allows cyclodextrins to extract cholesterol and/or deliver lipid ligands to cell membranes, resulting in significant interest in its potential as an antiviral therapeutic [41]. Furthermore, both processes have been observed to occur on a relatively fast timescale suggesting the presence of a membrane-bound intermediate step such as that described in Fig. 4B [42,43]. As with nsLTPs, the binding stoichiometries of cyclodextrins (~ 1 : 1) is significantly lower than that of AEG12, although their overall small size and simplicity might compensate for this [44,45]. While the AEG12–inhibitor complexes described in this work represent a significant improvement over the nMix counterparts, significant drawbacks remain – especially with regards to cell cytotoxicity in the case of GA-AEG12. This could be addressed through the use of more specialized hydrophobic viral inhibitor ligands such as 25-hydroxycholesterol or rigid amphipathic fusion inhibitors: strategies that may not be feasible with the smaller and more confined hydrophobic cavities of nsLTP or cyclodextrin scaffolds [46,47].

Through this work, we show that AEG12 can facilitate the delivery of hydrophobic viral fusion inhibitors. The resulting complexes displayed significantly enhanced therapeutic utility relative to both the free ligands and the naturally occurring nMix-AEG12 species against SARS CoV-2. We acknowledge that cytotoxicity and antiviral activity will vary depending on the targeted cell types (e.g. HEK vs. Vero) and therapeutic conditions. Nonetheless, the ability to modulate both these properties through the use of non-natural lipid ligands represents a novel approach to enhancing AEG12 antiviral activity and generating novel therapeutics to address a wide range of existing and emerging threats such as flaviviruses and HIV in addition to the ongoing COVID-19 pandemic.

Acknowledgements

We thank Dr Bob Petrovich for providing the cell lines and instrumentation employed in this study, and Dr Jeff Tucker, Erica Scappini, Rob Wine and Dr Agnes Janoshazi for their assistance with the fluorescence imaging. Finally, we thank Drs Negin Martin and

David Chen for their guidance and advice throughout this project. This research was supported by the Intramural Research Program of the NIH, National Institute of Environmental Health Sciences, Z01-ES102906 (GAM) and by the Intramural Research Program of the National Institute of Allergy and Infectious Diseases (BAPL).

Author contributions

ACYF, BAPL and GAM conceived and supervised the study, and designed experiments. ACYF and BAPL performed experiments and analysed data; ACYF and GAM wrote the manuscript, and BAPL made manuscript revisions.

Data accessibility

The data that support the findings of this study are available on request from the authors.

References

1 Shao L, Devenport M, Fujioka H, Ghosh A, Jacobs-Lorena M. Identification and characterization of a novel peritrophic matrix protein, ae-Aper50, and the microvillar membrane protein, AEG12, from the mosquito, *Aedes aegypti*. *Insect Biochem Mol Biol*. 2005;**35**(9):947–59. https://doi.org/10.1016/j.ibmb.2005.03.012

2 Colpitts TM, Cox J, Vanlandingham DL, Feitosa FM, Cheng G, Kurscheid S, et al. Alterations in the *Aedes aegypti* transcriptome during infection with West Nile, dengue and yellow fever viruses. *PLoS Pathog*. 2011;**7**(9):e1002189. https://doi.org/10.1371/journal.ppat.1002189

3 Sim S, Jupatanakul N, Ramirez JL, Kang S, Romero-Vivas CM, Mohammed H, et al. Transcriptomic profiling of diverse *Aedes aegypti* strains reveals increased basal-level immune activation in dengue virus-refractory populations and identifies novel virus-vector molecular interactions. *PLoS Negl Trop Dis*. 2013;**7**(7):e2295. https://doi.org/10.1371/journal.pntd.0002295

4 Saldaña MA, Etebari K, Hart CE, Widen SG, Wood TG, Thangamani S, et al. Zika virus alters the microRNA expression profile and elicits an RNAi response in *Aedes aegypti* mosquitoes. *PLoS Negl Trop Dis*. 2017;**11**(7):1–18. https://doi.org/10.1371/journal.pntd.0005760

5 Etebari K, Hedge S, Saldana MA, Widen SG, Wood TG, Asgari S, et al. Global transcriptome analysis of *Aedes aegypti* mosquitoes in response to zika virus infection. *mSphere*. 2017;**2**(6):e00456-17. https://doi.org/10.1128/JB.188.4.1648

6 Foo ACY, Thompson PM, Chen SH, Jadi R, Lupo B, DeRose EF, et al. The mosquito protein AEG12 displays both cytolytic and antiviral properties via a common lipid transfer mechanism. *Proc Natl Acad Sci USA*. 2021;**118**(11):e2019251118. https://doi.org/10.1073/pnas.2019251118

7 Foo ACY, Thompson PM, Perera L, Arora S, DeRose EF, Williams J, et al. Hydrophobic ligands influence the structure, stability, and processing of the major cockroach allergen Bla g 1. *Sci Rep*. 2019;**9**(1):1–12. https://doi.org/10.1038/s41598-019-54689-8

8 Mueller GA, Pedersen LC, Lih FB, Glesner J, Moon AF, Chapman MD, et al. The novel structure of the cockroach allergen Bla g 1 has implications for allergenicity and exposure assessment. *J Allergy Clin Immunol*. 2013;**132**(6):1420–6. https://doi.org/10.1016/j.jaci.2013.06.014

9 Matthews BW, Liu L. A review about nothing: are Apolar cavities in proteins really empty? *Protein Sci*. 2009;**18**(3):494–502. https://doi.org/10.1002/pro.61

10 Lee JY, Min K, Cha H, Shin DH, Hwang KY, Suh SW. Rice non-specific lipid transfer protein: the 1.6 Å crystal structure in the unliganded state reveals a small hydrophobic cavity. *J Mol Biol*. 1998;**276**(2):437–48. https://doi.org/10.1006/jmbi.1997.1550

11 Cheng CS, Chen MN, Liu YJ, Huang LY, Lin KF, Lyu PC. Evaluation of plant non-specific lipid-transfer proteins for potential application in drug delivery. *Enzyme Microb Technol*. 2004;**35**(6–7):532–9. https://doi.org/10.1016/j.enzmictec.2004.08.026

12 Foo ACY, Thompson PM, Mueller GA, Foo ACY, Thompson PM, Mueller GA. Removal and replacement of endogenous ligands from lipid-bound proteins and allergens. *J Vis Exp*. 2021;**168**:e61780. https://doi.org/10.3791/61780

13 Lü JM, Yan S, Jamaluddin S, Weakley SM, Liang Z, Siwak EB, et al. Ginkgolic acid inhibits HIV protease activity and HIV infection in vitro. *Med Sci Monit*. 2012;**18**(8):293–8. https://doi.org/10.12659/MSM.883261

14 Campos D, Navarro S, Llamas-González YY. Broad antiviral activity of Ginkgolic acid against chikungunya, Mayaro, una, and zika viruses. *Viruses*. 2020;**12**(4):449. https://doi.org/10.3390/v12040449

15 Borenstein R, Hanson BA, Markosyan RM, Gallo ES, Narasipura SD, Bhutta M, et al. Ginkgolic acid inhibits fusion of enveloped viruses. *Sci Rep*. 2020;**10**(1):1–12. https://doi.org/10.1038/s41598-020-61700-0

16 Katz DH, Marcelletti JF, Khalil MH, Pope LE, Katz LR. Antiviral activity of 1-Docosanol, an inhibitor of lipid-enveloped viruses including herpes simplex. *Proc Natl Acad Sci USA*. 1991;**88**(23):10825–9. https://doi.org/10.1073/pnas.88.23.10825

17 Gunther-Ausborn S, Praetor A, Stegmann T. Inhibition of influenza-induced membrane fusion by

lysophosphatidylcholine. *J Biol Chem*. 1995;**270**(49):29279–85. https://doi.org/10.1074/jbc.270.49.29279

18 Ohki S, Baker GA, Page PM, McCarty TA, Epand RM, Bright FV. Interaction of influenza virus fusion peptide with lipid membranes: effect of lysolipid. *J Membr Biol*. 2006;**211**(3):191–200. https://doi.org/10.1007/s00232-006-0862-z

19 Hoekstra D, de Boer T, Klappe K, Wilschut J. Fluorescence method for measuring the kinetics of fusion between biological membranes. *Biochemistry*. 1984;**23**(24):5675–81. https://doi.org/10.1021/bi00319a002

20 Stegmann T, Wey J, Bartoldus I, Schoen P, Bron R, Ortiz A, et al. Evaluation of viral membrane fusion assays. Comparison of the octadecylrhodamine dequenching assay with the pyrene excimer assay. *Biochemistry*. 1993;**32**(42):11330–7. https://doi.org/10.1021/bi00093a009

21 Parasassi T, Krasnowska EK, Bagatolli L, Gratton E. Laurdan and Prodan as polarity-sensitive fluorescent membrane probes. *J Fluoresc*. 1998;**8**(4):365–73.

22 Schindelin J, Arganda-Carreras I, Frise E, Kaynig V, Longair M, Pietzsch T, et al. Fiji: an open-source platform for biological-image analysis. *Nat Methods*. 2012;**9**(7):676–82. https://doi.org/10.1038/nmeth.2019

23 Liu X, Luongo C, Matsuoka Y, Park HS, Santos C, Yang L, et al. A single intranasal dose of a live-attenuated parainfluenza virus-vectored SARS-CoV-2 vaccine is protective in hamsters. *Proc Natl Acad Sci USA*. 2021;**118**(50):1–11. https://doi.org/10.1073/pnas.2109744118

24 Bhutta MS, Sausen DG, Gallo ES, Dahari H, Doncel GF, Borenstein R. Ginkgolic acid inhibits coronavirus strain 229e infection of human epithelial lung cells. *Pharmaceuticals*. 2021;**14**(10):1–11. https://doi.org/10.3390/ph14100980

25 Pope LE, Marcelletti JF, Katz LR, Lin JY, Katz DH, Parish ML, et al. The anti-herpes simplex virus activity of n-Docosanol includes inhibition of the viral entry process. *Antiviral Res*. 1998;**40**(1–2):85–94. https://doi.org/10.1016/S0166-3542(98)00048-5

26 Hall J. A simple model for determining affinity from irreversible thermal shifts. *Protein Sci*. 2019;**28**(10):1880–7. https://doi.org/10.1002/pro.3701

27 Stiasny K, Heinz FX. Effect of membrane curvature-modifying lipids on membrane fusion by tick-borne encephalitis virus. *J Virol*. 2004;**78**(16):8536–42. https://doi.org/10.1128/jvi.78.16.8536-8542.2004

28 Høyrup P, Davidsen J, Jørgensen K. Lipid membrane partitioning of lysolipids and fatty acids: effects of membrane phase structure and detergent chain length. *J Phys Chem B*. 2001;**105**(13):2649–57. https://doi.org/10.1021/jp003631o

29 Pantusa M, Bartucci R, Marsh D, Sportelli L. Shifts in chain-melting transition temperature of liposomal membranes by polymer-grafted lipids. *Biochim Biophys Acta*. 2003;**1614**(2):165–70. https://doi.org/10.1016/S0005-2736(03)00171-8

30 Cevc G. How membrane chain-melting phase-transition temperature is affected by the lipid chain asymmetry and degree of unsaturation: an effective chain-length model. *Biochemistry*. 1991;**30**(29):7186–93. https://doi.org/10.1021/bi00243a021

31 Chen W, Duša F, Witos J, Ruokonen SK, Wiedmer SK. Determination of the main phase transition temperature of phospholipids by nanoplasmonic sensing. *Sci Rep*. 2018;**8**(1):1–11. https://doi.org/10.1038/s41598-018-33107-5

32 Kraske WV, Mountcastle DB. Effects of cholesterol and temperature on the permeability of dimyristoylphosphatidylcholine bilayers near the chain melting phase transition. *Biochim Biophys Acta*. 2001;**1514**(2):159–64. https://doi.org/10.1016/S0005-2736(01)00379-0

33 Plemel JR, Michaels NJ, Weishaupt N, Caprariello AV, Keough MB, Rogers JA, et al. Mechanisms of lysophosphatidylcholine-induced demyelination: a primary lipid disrupting myelinopathy. *Glia*. 2018;**66**(2):327–47. https://doi.org/10.1002/glia.23245

34 Kim YL, Im YJ, Ha NC, Im DS. Albumin inhibits cytotoxic activity of lysophosphatidylcholine by direct binding. *Prostaglandins Other Lipid Mediat*. 2007;**83**(1–2):130–8. https://doi.org/10.1016/j.prostaglandins.2006.10.006

35 Ojala PJ, Hirvonen TE, Hermansson M, Somerharju P, Parkkinen J. Acyl chain-dependent effect of lysophosphatidylcholine on human neutrophils. *J Leukoc Biol*. 2007;**82**(6):1501–9. https://doi.org/10.1189/jlb.0507292

36 Abreu MSC, Luis MBBL, Moreno MJ, Vaz WLC. Binding of a fluorescent lipid amphiphile to albumin and its transfer to lipid bilayer membranes. *Biophys J*. 2003;**84**(1):386–99. https://doi.org/10.1016/S0006-3495(03)74859-0

37 Estronca LMBB, Moreno MJ, Laranjinha JAN, Almeida LM, Vaz WLC. Kinetics and thermodynamics of lipid amphiphile exchange between lipoproteins and albumin in serum. *Biophys J*. 2005;**88**(1):557–65. https://doi.org/10.1529/biophysj.104.047050

38 Nichols JW. Kinetics of fluorescent-labeled phosphatidylcholine transfer between nonspecific lipid transfer protein and phospholipid vesicles. *Biochemistry*. 1988;**27**:1889–96.

39 Cheng CS, Samuel D, Liu YJ, Shyu JC, Lai SM, Lin KF, et al. Binding mechanism of nonspecific lipid transfer proteins and their role in plant defense. *Biochemistry*. 2004;**43**(43):13628–36. https://doi.org/10.1021/bi048873j

40 Pato C, Le Borgne M, Le Baut G, Le Pape P, Marion D, Douliez JP. Potential application of plant lipid

transfer proteins for drug delivery. *Biochem Pharmacol*. 2001;**62**(5):555–60. https://doi.org/10.1016/S0006-2952(01)00708-0

41 Garrido PF, Calvelo M, Blanco-González A, Veleiro U, Suárez F, Conde D, et al. The Lord of the NanoRings: cyclodextrins and the battle against SARS-CoV-2. *Int J Pharm*. 2020;**588**:119689. https://doi.org/10.1016/j.ijpharm.2020.119689

42 Sugiura T, Ikeda K, Nakano M. Kinetic analysis of the methyl-β-cyclodextrin-mediated Intervesicular transfer of pyrene-labeled phospholipids. *Langmuir*. 2016;**32**(51):13697–705. https://doi.org/10.1021/acs.langmuir.6b03515

43 Beseničar MP, Bavdek A, Kladnik A, Maček P, Anderluh G. Kinetics of cholesterol extraction from lipid membranes by methyl-β-cyclodextrin-a surface plasmon resonance approach. *Biochim Biophys Acta*. 2008;**1778**(1):175–84. https://doi.org/10.1016/j.bbamem.2007.09.022

44 Ondo D. Thermodynamic study on complexation of long-chain fatty acid anions with α-cyclodextrin in water. *J Mol Liq*. 2020;**311**:113172. https://doi.org/10.1016/j.molliq.2020.113172

45 Skoulika SG, Georgiou CA, Polissiou MG. Interaction of β-cyclodextrin with unsaturated and saturated straight chain fatty acid anions studied by phenolphthalein displacement. *J Incl Phenom Macrocycl Chem*. 1999;**34**(1):85–96. https://doi.org/10.1023/A:1008080619470

46 Zu S, Deng YQ, Zhou C, Li J, Li L, Chen Q, et al. 25-Hydroxycholesterol is a potent SARS-CoV-2 inhibitor. *Cell Res*. 2020;**30**:1043–5. https://doi.org/10.1038/s41422-020-00398-1

47 St. Vincent MR, Colpitts CC, Ustinov AV, Muqadas M, Joyce MA, Barsby NL, et al. Rigid amphipathic fusion inhibitors, small molecule antiviral compounds against enveloped viruses. *Proc Natl Acad Sci USA*. 2010;**107**(40):17339–44. https://doi.org/10.1073/pnas.1010026107